

Microscopic Two-uid Theory of Rotational Constants of the OCS-H_2 Complex in ^4He Droplets

Yongkyung Kwon^{1,2} and K. Birgitta Whaley²

¹Department of Physics, Konkuk University, Seoul 143-701, Korea and

²Department of Chemistry and Kenneth S. Pitzer Center for Theoretical Chemistry,
University of California, Berkeley, CA 94720, USA

(Dated: March 22, 2024)

We present a microscopic quantum analysis for rotational constants of the OCS-H_2 complex in helium droplets using the local two-uid theory in conjunction with path integral Monte Carlo simulations. Rotational constants are derived from effective moments of inertia calculated assuming that motion of the H_2 molecule and the local non-superfluid helium density is rigidly coupled to the molecular rotation of OCS and employing path integral methods to sample the corresponding H_2 and helium densities. The rigid coupling assumption for $\text{H}_2\text{-OCS}$ is calibrated by comparison with exact calculations of the free OCS-H_2 complex. The presence of the H_2 molecule is found to induce a small local non-superfluid helium density in the second solvation shell which makes a non-negligible contribution to the moment of inertia of the complex in helium. The resulting moments of inertia for the OCS-H_2 complex embedded in a cluster of 63 helium atoms are found to be in good agreement with experimentally measured values in large helium droplets. Implications for analysis of rotational constants of larger complexes of OCS with multiple H_2 molecules in helium are discussed.

PACS numbers: 36.40.-c, 36.40.Mr, 67.40.-w, 67.40.Yv

I. INTRODUCTION

Helium droplets are known to provide an attractively convenient environment for synthesis of weakly bound, metastable, or other unusual complexes¹. The low temperature of these droplets ($0.15\text{--}0.4\text{ K}$), their liquid nature, and their weak interaction with impurity species render them ideal matrix hosts for weakly bound complexes. Formation of such complexes is facilitated by the now standard pick-up technique² in which foreign species are absorbed by the droplet in a pick-up chamber. Sequential use of such pick-up allows assembly of a variety of complexes and aggregates of atoms and molecules. In recent years this synthetic potential of helium clusters has been demonstrated with synthesis of water clusters,³ of metal clusters,^{4,5} of metal-adsorbate clusters,⁶ and of chains of HCN ,⁷ all in the ultra-cold environment of a helium droplet. In several of these instances high resolution spectroscopy of the embedded clusters has shown that metastable isomers of conformations not seen for the corresponding clusters in the gas phase are formed in helium. This indicates that although weak, the effect of helium solvation is non-negligible in determining the structure of some complexes, in particular those formed from polar constituents.

Complexes of molecules with molecular hydrogen constitute a special type of complex whose formation and behavior in helium droplets is currently of great interest. The possibility of finding a superfluid state of molecular hydrogen provides an additional motivation beyond that of merely forming the complexes and analyzing the effect of helium solvation on their structure. Molecular hydrogen superfluidity is most likely to be found for the $j = 0$ state of H_2 , i.e., para- H_2 , the lightest bosonic molecule of the hydrogen isotopes. We shall restrict ourselves to

para- H_2 in this work, and for simplicity refer to it as H_2 . Helium will in all cases be taken as the boson isotope, ^4He . A number of significant experimental results have been obtained for $\text{OCS}(\text{H}_2)_M$ complexes in recent years. Ref. 8 showed that for $M \leq 11$ there exist spectral anomalies which are consistent with the existence of a superfluid state of the H_2 molecules. Existence of this superfluid state of molecular hydrogen in a nanoscale system has recently been confirmed by path integral calculations and shown to have an onset at a temperature of 0.3 K for hydrogen clusters around OCS .⁹ Additional spectroscopic studies have been made for $M = 1\text{--}8$ in helium droplets and analyzed in terms of rigidly coupled models of the $\text{OCS}(\text{H}_2)_M$ complexes.^{10,11} For the smallest $M = 1$ complex of OCS-H_2 , the corresponding gas phase spectroscopy has recently been measured and analyzed in Ref. 12. This smallest complex provides a reference point for theoretical analysis of this and all larger clusters with $M > 1$ in helium.

In this work we undertake a detailed theoretical analysis of the $M = 1$ complex OCS-H_2 in droplets of ^4He , using path integral methodology and the local two-uid theory.¹³ We make path integral Monte Carlo calculations of the complex in clusters of $N = 63$ helium atoms. This size is large enough to provide a complete first solvation shell around the OCS molecule ($N = 20$)¹⁴ that has a robust and compact structure which is independent of further increases in N . Both hydrogen molecule and helium atoms are described quantum mechanically, with full permutation exchange symmetry of the helium component incorporated. We compute the local non-superfluid helium solvation density induced by the OCS-He and $\text{H}_2\text{-He}$ interactions. Comparison of this non-superfluid density around OCS in pure $^4\text{He}_{64}$ and around OCS-H_2 in $^4\text{He}_{63}$ shows that the H_2 molecule in-

duces a small non-superfluid density around itself in the second solvation shell of helium as well as in the first shell.

We evaluate the effective moment of inertia of the OCS molecule assuming that the H_2 molecule is rigidly coupled to the molecular rotation and employing the microscopic two-fluid theory of Ref. 13 to evaluate the contribution from the helium solvation density. The assumption of rigid coupling of H_2 to the molecular rotation is tested by an evaluation of the rotational constants of free (gas phase) OCS- H_2 and by comparison of these with the experimental values measured in Ref. 12. This comparison, made with interaction potentials¹⁵ that have been previously calibrated for OCS- H_2 by exact bound state calculations,¹⁶ shows that the free OCS- H_2 complex can be very accurately described with a rigid coupling model. This free complex is planar, with mass distribution corresponding to an asymmetric top. Excellent agreement of the calculated moments of inertia with experimental values is found. The free complex calculations are followed by a local two-fluid analysis of the response of the solvating helium density to rotation of this OCS- H_2 complex, to obtain estimates for the helium contribution to all three moments of inertia in helium droplets. The average moment of inertia resulting from this analysis incorporating both first and second shell complex-induced non-superfluid helium densities is in excellent agreement with the corresponding experimentally measured value in helium droplets, with an accuracy of 4%. The calculated inertial defect indicates a non-planar mass distribution of the total helium-solvated complex, in agreement with the experimental measurements. Comparison of individual moments of inertia with their corresponding experimental values shows somewhat larger deviations of 10 – 20%. The smaller accuracy of the individual moments of inertia can be ascribed to limitations of the local non-superfluid estimators used here in distinguishing accurately between rotations around different axes.

Such quantitative agreement of the moments of inertia and of the corresponding rotational constants with experimental measurements implies that the underlying model of an OCS molecule rotating with a rigidly coupled H_2 molecule and a rigidly coupled local non-superfluid density of helium provides an accurate description for the low rotational states of the OCS- H_2 complex that are accessed by spectroscopic measurements. Given that high quality interaction potentials calibrated by experimental measurements of the free OCS-He and OCS- H_2 complexes are employed here, we can take the agreement between these results for the hydrogen complex of OCS embedded in helium with experiment as providing further evidence for the accuracy of the local two-fluid model of quantum solvation and superfluid response to rotational motion around heavy molecules.^{13,17}

The structure of the rest of the paper is as follows. In Section II we summarize the path integral methodology used for these calculations with both helium and hydrogen treated quantum mechanically. In Section III

we describe the interaction potentials and present the various calibration calculations for the gas phase OCS- H_2 complex that provide a validation of our assumption that at low energies the dynamics of the H_2 molecule are rigidly coupled to the molecular rotation. Section IV then presents the results of the full path integral calculations and microscopic two-fluid analysis for the OCS- H_2 complex when embedded in helium clusters. We conclude in Section V with a summary and brief discussion of implications for larger complexes of OCS(H_2)_M in helium.

II. METHODOLOGY

In this work the OCS molecule is treated as fixed and non-rotating. These restrictions are convenient because of the greater computational cost associated with the quantum treatment of the additional H_2 molecule. The consequences of these restrictions are not severe for the two-fluid analysis, as the following arguments indicate. Previous studies have shown that for heavy molecules the helium solvation density around an embedded molecule is not significantly affected by the molecule translation motion,^{18,19} but that there is a significant decrease in the angular modulation of this solvation density when the molecular rotational degrees of freedom are incorporated.^{14,20} Very recent path integral studies that incorporate all molecular translational and rotational degrees of freedom have shown that the integrated local non-superfluid density is insensitive to this modulation and that the moment of inertia contributions from the local non-superfluid may be accurately estimated from calculations made for a non-rotating and non-translating OCS.²¹ Therefore we shall employ a non-rotating OCS molecule here and postpone investigation of the detailed effects of OCS rotational and translational motions to future work.

For the interaction potentials between the three different particles involved (para- H_2 , He, and OCS), we use a sum of pair potentials consisting of H_2 -He,²² He-He,²³ OCS- H_2 ,¹⁵ and OCS-He,²⁴ terms. The para-hydrogen molecules are treated as spherical particles like the helium atoms. This is a well justified approximation at these low temperatures because of the large rotational constant and nearly isotropic ground-state electronic configuration of H_2 . Consequently, we average the three-dimensional *ab initio* OCS- H_2 potential which has recently been computed by Higgins et al. with fourth-order Møller-Plesset (MP4) perturbation theory,¹⁵ over the orientation of the H_2 molecule. This results in a two-dimensional representation of the OCS- H_2 interaction that has a very similar topology to the previously reported MP4 OCS-He potential.²⁴ Contour plots of the two potentials are shown in Figure 1. It is evident that the OCS- H_2 potential has its global minimum at approximately the same location as the OCS-He potential, but possesses a significantly deeper value. For OCS- H_2 , the global minimum is 208 K, located at $r = 3.35$ Å and

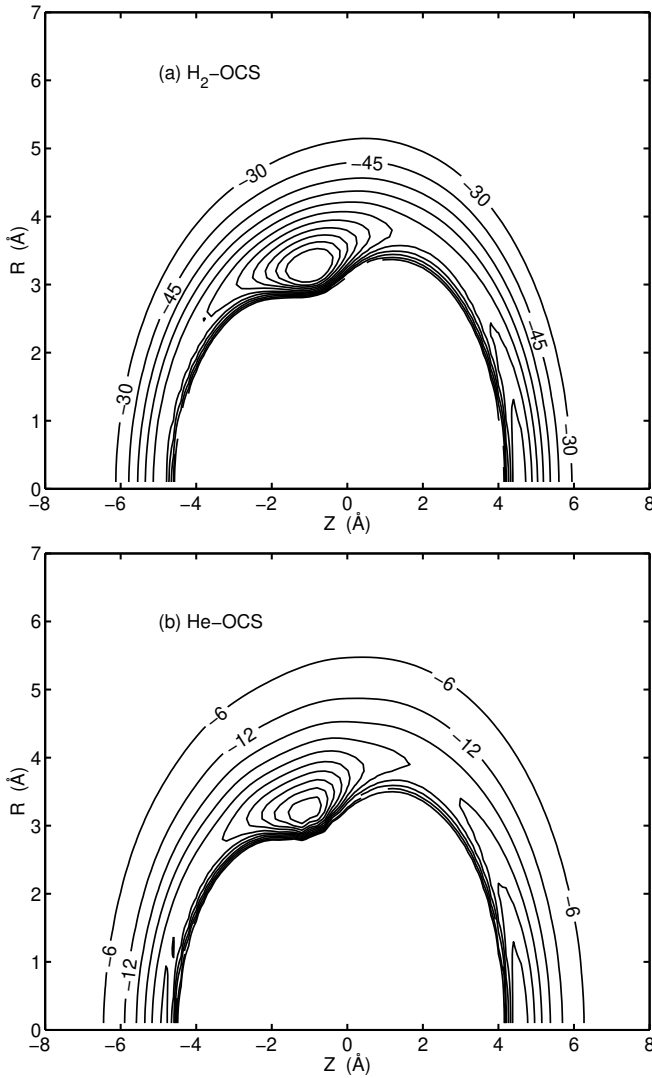


FIG. 1: Contour plots of the $\text{H}_2\text{-OCS}$ and He-OCS potentials, shown as a function of the cylindrical coordinates (Z, R) , where Z is the coordinate along the axis passing through the OCS molecule and R is the radial distance from the OCS molecular axis. The origin is set at the center of mass of the OCS and the molecule is oriented as O-C-S from Z to $+Z$. Contours are shown in increments of 15 K for the $\text{H}_2\text{-OCS}$ and 6 K for the He-OCS potential, respectively.

$= 106$, where r is the distance from the OCS center of mass and θ the polar angle measured from the sulfur side of the OCS molecular axis. For OCS-He, the global minimum is 65.3 K and is located at $r = 3.38$ Å, $\theta = 108^\circ$. All calculations described here employ these two MP4 potentials for the interaction of OCS with H_2 and He. For the $\text{H}_2\text{-He}$ and He-He interactions we use the empirical potential proposed by van den Bergh and Schouten,²² and the semi-empirical potential of Aziz et al.,²³ respectively.

We now have the following system Hamiltonian for the

$\text{H}_2\text{-OCS}$ complex inside the $^4\text{He}_N$ cluster:

$$H = \frac{\hbar^2}{2m_{\text{H}_2}} \nabla_0^2 + \sum_{i=1}^N \frac{\hbar^2}{2m_{\text{He}}} \nabla_i^2 + \sum_{i<j} V_{\text{He-He}}(r_{ij}) + \sum_{i=1}^N V_{\text{H}_2\text{-He}}(r_{0i}) + V_{\text{H}_2\text{-OCS}}(\mathbf{r}_0) + \sum_{i=1}^N V_{\text{He-OCS}}(\mathbf{r}_i): \quad (1)$$

Here m_{H_2} (m_{He}) is the mass of a hydrogen molecule (helium atom) and \mathbf{r}_0 is the position vector of the hydrogen molecule in a (space fixed, for a non-rotating molecule) frame centered on the OCS molecule.

To study the OCS- H_2 complex and its helium solvation structure we employ here the path integral Monte Carlo (PIMC) technique. This approach allows us to make the quantitative analysis of superfluidity in the helium environment that is required for the local two-fluid theory. The main elements of the PIMC technique have been described in Ref. 25 and its adaptation to molecule-doped helium clusters detailed in Ref. 19. We give here only a brief summary, with methodological details that are specific to the OCS- H_2 and its helium surroundings. The thermal density matrix is given by

$$(\mathbf{R}; \mathbf{R}^0;) = \langle \mathbf{R} | e^{-\beta H} | \mathbf{R}^0 \rangle; \quad (2)$$

with $\beta = 1/k_B T$, \mathbf{R} a $3(N+1)$ -dimensional vector, $\mathbf{R} = (\mathbf{r}_0; \mathbf{r}_1; \dots; \mathbf{r}_N)$, and H equal to the Hamiltonian, Eq. (1), for an H_2 molecule and N helium atoms in the external field provided by the stationary OCS molecule. In order to incorporate the bosonic symmetry of the ^4He atoms, the density matrix is symmetrized by summing all permutations P amongst the N helium atoms:

$$\mathbf{B}(\mathbf{R}; \mathbf{R}^0;) = \frac{1}{N!} \sum_P (\mathbf{R}; P \mathbf{R}^0;); \quad (3)$$

Since the density matrix of a interacting quantum system is generally not known at a low temperature T , it is replaced in the Feynman path integral representation with a product of L higher-temperature density matrices, resulting in the discrete time path integral:

$$\mathbf{B}(\mathbf{R}; \mathbf{R}^0;) = \int \prod_{i=1}^L d\mathbf{R}_i \int \prod_{i=1}^L d\mathbf{R}_i \mathbf{B}(\mathbf{R}; \mathbf{R}_1;) \mathbf{B}(\mathbf{R}_1; \mathbf{R}_2;) \dots \mathbf{B}(\mathbf{R}_L; \mathbf{R}^0;); \quad (4)$$

Here $\tau = \beta/L$ constitutes the imaginary time step defining this discrete representation of the path integral. At sufficiently high temperatures $1/T$, or equivalently, at sufficiently small time steps τ , the density matrix $\mathbf{B}(\mathbf{R}; \mathbf{R}^0;)$ can be approximated by a product of the free particle propagator and an interaction term. For the spherical He-He and $\text{H}_2\text{-He}$ interactions, the pair-product form of the exact two-body density matrices can be used, and a matrix squaring methodology employed to achieve accurate grid representation of these.²⁵

The anisotropic He-OCS and H₂-OCS interactions are treated here within the primitive approximation.¹⁹ From our previous study of OCS-doped He_N clusters, we have found that a time step of $\tau = 80$ K is required to get converged helium density profiles around the molecule with this approximation for the high-temperature density matrix.²⁶ In order to make a simultaneous calculation of the sum over N -particle permutations in Eq. (3) together with the multi-dimensional integration over the position coordinates in the discrete time path integral, Eq. (4), we employ a stochastic process which samples the discrete paths $\{R; R_1; R_2; \dots; R_{L-1}; P; R^0\}$ with probability density proportional to $(R; R_1; \dots) (R_1; R_2; \dots) \dots L(R; P; R^0; \dots)$. This sampling is performed by the generalized Metropolis sampling algorithm of Pollock and Ceperley.²⁷ A detailed description of this algorithm is provided in Refs. 28, 25 and 19. The thermal average of any observable \hat{O} can then be determined by computing an arithmetic average of $\langle R^0 | \hat{O} | R \rangle$ over the paths sampled.

One of the advantages of using the path integral approach is that it allows a quantitative estimate to be made of the superfluidity of bosonic systems such as ⁴He and para-H₂ clusters as a function of temperature. Within the Feynman path integral analysis, the global superfluid fraction that is defined as the linear response of the bosonic system to classical rotation of its boundaries can be evaluated by an estimator written in terms of the projected area of the Feynman paths²⁹:

$$f_{ij}^s = \frac{4m^2 \hbar A_i A_j i k_B T}{h^2 I_{ij}^{cl}} \quad (5)$$

Here A_i is the area of a Feynman path projected onto a plane perpendicular to the axis \hat{x}_i , and I^{cl} is the classical moment of inertia tensor. This estimator yields a non-negligible value only when exchange-coupled paths are comparable to the size of the system. One problem that arises when applying this global superfluid estimator to analysis of doped helium clusters is that it does not give information about the local perturbation of superfluidity due to the presence of an impurity. However, it is precisely the local perturbation of the superfluid that determines the dynamic response of the helium to the rotation of an embedded molecule,^{13,17} so that a local analysis of superfluidity in the solvating helium density is required. Another possible issue with this estimator is that it provides a measure of the superfluid response to classical rotation of a boundary as the rotation speed goes to zero, which does not map to the quantized rotation of a molecule. While this may not be very significant for analysis of the molecule-induced local non-superfluid density, given that this appears to be independent of the effects of molecular rotation,²¹ it should be borne in mind when interpreting the meaning of the local superfluid density.

In order to estimate the local superfluid fraction around an impurity molecule, we compute here the density distribution of helium atoms participating in permutation exchanges which result in paths that are long

compared to the system size. In our previous studies of SF₆-He_N and OCS-He_N clusters,^{13,17,26} we found that a robust local superfluid distribution in the first shell region could be computed for $N = 50$ by counting the exchange paths involving more than six helium atoms. The result is robust to the precise value of this cut-off, i.e., similar results are obtained with five- or seven-atom exchange paths. As pointed out in Ref. 17, this local estimator based purely on the exchange path length does not reflect the tensorial nature of the superfluid response that is predicted from the linear response definition, Eq. (5). An alternative local estimator that is derived from decomposition of Eq. (5) into contributions from small cells has recently been proposed in Ref. 30. This alternative estimator does possess the correct tensorial nature of the linear superfluid response, but unfortunately it is subject to extremely large fluctuations. To obtain meaningful values within small regions such as the first solvation shell of OCS would require an extremely high computational effort. (The application of this estimator in Ref. 30 employed cylindrical averaging over the length of a linear chain of three HCN molecules, which reduces the fluctuations.) Thus, in order to make a microscopic analysis of the effect of the surrounding helium on the moment of inertia of the embedded H₂-OCS complex, we employ here the original local estimator of superfluid fraction employing long exchange path length.

III. STRUCTURE AND ROTATIONAL CONSTANTS OF FREE OCS-H₂

We first performed a PIMC calculation on the free H₂-OCS complex, i.e., without any helium atom present. Figure 2 shows the density distribution of the single hydrogen molecule around OCS in the absence of helium. The hydrogen molecule is clearly located at and around the global minimum of H₂-OCS potential. Its average position is $r = 3.63 \pm 0.33$ Å, $\theta = 106.5 \pm 8.5^\circ$. The uncertainties are evaluated as the fluctuations $\Delta x =$

$\sqrt{\langle x^2 \rangle - \langle x \rangle^2}$ which provide a measure of the widths of the single peak in the density distribution. These PIMC values of r and θ extracted from the finite temperature density distributions are very similar to the corresponding values obtained from ground state expectation values, namely $r = 3.704$ Å and $\theta = 105.7^\circ$.¹⁶ The average hydrogen position defines an average center of mass of the H₂-OCS complex. Transforming to the complex body-fixed frame, yields the average coordinates $r^0 = 3.51 \pm 0.33$ Å and $\theta^0 = 106.5 \pm 8.5^\circ$, where r^0 is the distance from the complex center of mass and θ^0 the polar angle from the complex body-fixed z -axis which is defined to be parallel to the OCS molecular axis. We see that there is only a very slight displacement of the center of mass away from the OCS center of mass (0.117 Å) as a result of complexing with the light hydrogen molecule.

We compute the moment of inertia tensor of this complex assuming that the hydrogen is rigidly attached to the

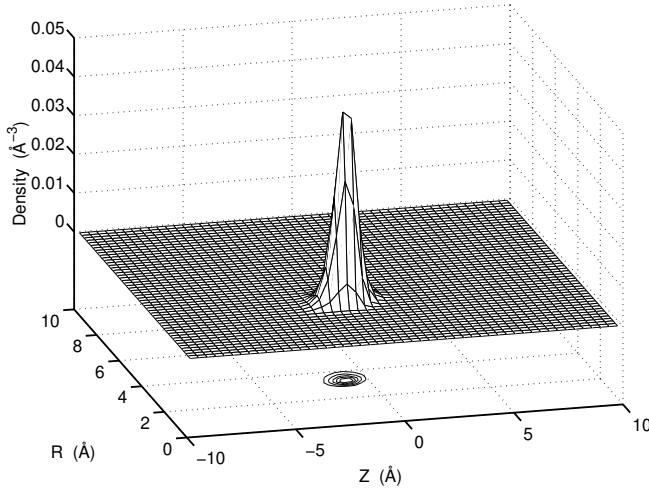


FIG. 2: Density of H_2 in the free $OCS-H_2$ complex, shown in the cylindrical coordinates Z and R with origin at the OCS center of mass (see Figure 1).

OCS molecular rotation. Thus, at each imaginary time configuration we evaluate the instantaneous moment of inertia tensor in the (instantaneous) body-fixed frame of the complex which is centered on the center of mass of the complex with z -axis parallel to the molecular axis, x -axis perpendicular to this and in the $OCS-H_2$ plane, and y -axis mutually perpendicular to both x - and z -axes. Averaging over the path integral yields the tensor components

$$I_{ij} = [I_0]_{ij} + m_{H_2} h(r^2_{ij} - x_i x_j) \delta_{ij}; \quad (6)$$

where I_0 is the gas-phase moment of inertia tensor of free OCS , and the coordinates x_i are the components of the hydrogen position vector \mathbf{r} in the body-fixed frame. Note that the y -axis is a principal axis of the moment of inertia tensor and corresponds to axis \hat{c} below. We then diagonalize this tensor to obtain the three principal values for the moments of inertia, namely I_a , I_b , and I_c , and their corresponding principal axes \hat{a} , \hat{b} , and \hat{c} . We obtain the rotational constants of the complex from the inverse of the principal moments of inertia, e. g., $A = h^2/2I_a$.

The resulting moments of inertia, I_a , I_b , and I_c , and rotational constants A , B , and C are listed in Table I (PIMC (1)). The corresponding principal axes are: \hat{a} in the xz -plane rotated an angle α away from the body-fixed z -axis, \hat{b} perpendicular to this and within the same plane, and \hat{c} perpendicular to the xz -plane. The angle α is also listed in Table I. Figure 3 shows the relation between the body-fixed and principal axes of the complex. To assess the effect of the displacement of the center of mass away from the OCS molecule, we have also calculated the moment of inertia tensor and corresponding values of A , B , C , and α in a body-fixed frame that is centered at the OCS center of mass. These values are shown in Table I as PIMC (2). The displacement of the center of mass

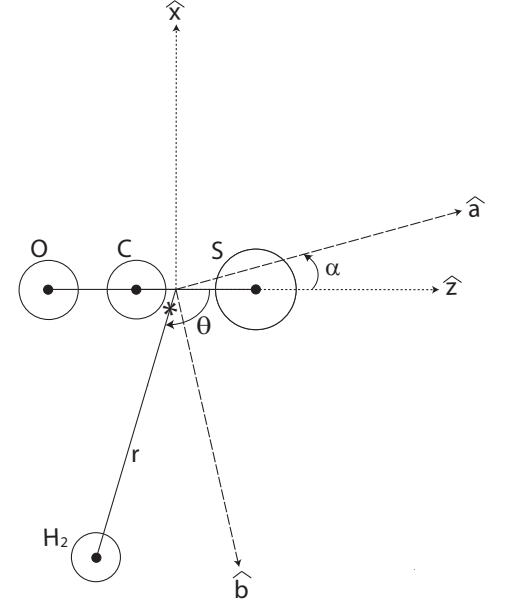


FIG. 3: Schematic of the geometry and principal axes of the free $OCS-H_2$ complex. \hat{x} and \hat{z} denote the coordinate system in the body-fixed frame centered on the OCS molecule center of mass. The principal axes (\hat{a} ; \hat{b}) are shown here in this frame. The third coordinate \hat{y} and principal axis \hat{c} are perpendicular to the plane of the paper, with \hat{y} directed out of the page and \hat{c} into the page. The asterisk denotes the complex center of mass, located at 0.117 Å away from the molecule center of mass on the $OCS-H_2$ axis. Distances are shown to scale.

away from the OCS axis is seen to have only small effects on the rotational constants and the angle α . The PIMC results are compared in Table I with i) the values obtained from exact calculations employing close-coupling and descendant-weighted diffusion Monte Carlo calculations with the same H_2-OCS potential¹⁶, and ii) recent experimental measurements.

We discuss first the comparison with the exact calculations. This comparison allows us to assess the accuracy of the rigid coupling assumption for H_2 . The PIMC rotational constants are seen to be in excellent agreement (1%) with the values derived from converged energy levels obtained with the close-coupling BOUND program.³¹ Consequently we can conclude that the assumption that H_2 is rigidly coupled to the OCS molecular rotation is indeed very accurate for $OCS-H_2$. This is not the case for the analogous $OCS-He$ complex, as is investigated with other methods and discussed in more detail in Ref. 16.

TABLE I: Moments of inertia (in $\text{amu } \text{\AA}^2$) and rotational constants (in cm^{-1}) of the free OCS-H_2 complex. θ is the angle between the OCS molecular axis and the \hat{a} principal axis. PIMC (1) is obtained with the body-fixed frame centered at the true center of mass of the complex. PIMC (2) is obtained with the approximation that the body-fixed frame is centered at the OCS center of mass. The experimental value of θ was estimated from the measured intensity ratios in Ref. 12, $\theta = \arctan(b/a)$. The exact results in column 3 derive from rotational energy levels obtained from the BOUND program,³¹ (rotation constants and moments of inertia) and from a ground state average of the moment of inertia evaluated with exact densities from diffusion Monte Carlo calculations (θ).¹⁶

	PIMC (1)	PIMC (2)	EXACT ^{16,31}	Expt. ¹²
I_a	21.93 (2)	22.84 (2)	22.29	22.14
I_b	85.87 (2)	86.39 (2)	84.50	84.25
I_c	108.26 (2)	109.24 (2)	109.28	109.78
	5.63	6.29	5.83	7.97
A	0.7679 (7)	0.742 (3)	0.7554	0.7607
B	0.1961 (1)	0.1941 (5)	0.1993	0.1999
C	0.1556 (1)	0.1537 (5)	0.1541	0.1534

The experimental measurements in the right hand column of Table I derive from a recent experimental characterization of the free OCS-H_2 complex by infra-red spectroscopy.¹² From spectral transitions between low-lying energy levels of the complex, it was determined that OCS-H_2 is an asymmetric rotor at low energies. Table I shows that the experimentally measured rotational constants (column 3) are in excellent agreement (within 0.5%) with the values obtained from the exact BOUND calculations (column 2). This confirms that the OCS-H_2 interaction potential used here¹⁵ is very accurate, at least in the region around its global minimum where the single hydrogen is predominantly located.

We have now confirmed both the accuracy of both the OCS-H_2 potential and the rigid coupling approximation for the OCS-H_2 complex. Given these two calibrations, we can proceed to directly compare the PIMC rotational constants (column 1, PIMC (1)) with the experimental values (column 3). The agreement here is also excellent (0.5–3%). The rotational constants A and C , the angle θ , and the free OCS rotational constant ($b = 0.20285 \text{ cm}^{-1}$)³² can be used with the ball-and-stick model of Hayman et al.³³ to obtain an independent estimate of the structural parameters r^0 , r_{bs}^0 and θ^0 . We note that the experimentally derived estimates for the ball-and-stick parameters, $r_{bs} = 3.719 \text{ \AA}$, $r_{bs}^0 = 110.8^\circ$,¹² lie within the width of the hydrogen density peak in Figure 2.

The consistently close agreement of the PIMC results for all spectroscopic and structural quantities with the corresponding experimental quantities therefore allow us to conclude that a rigid coupling analysis made with path

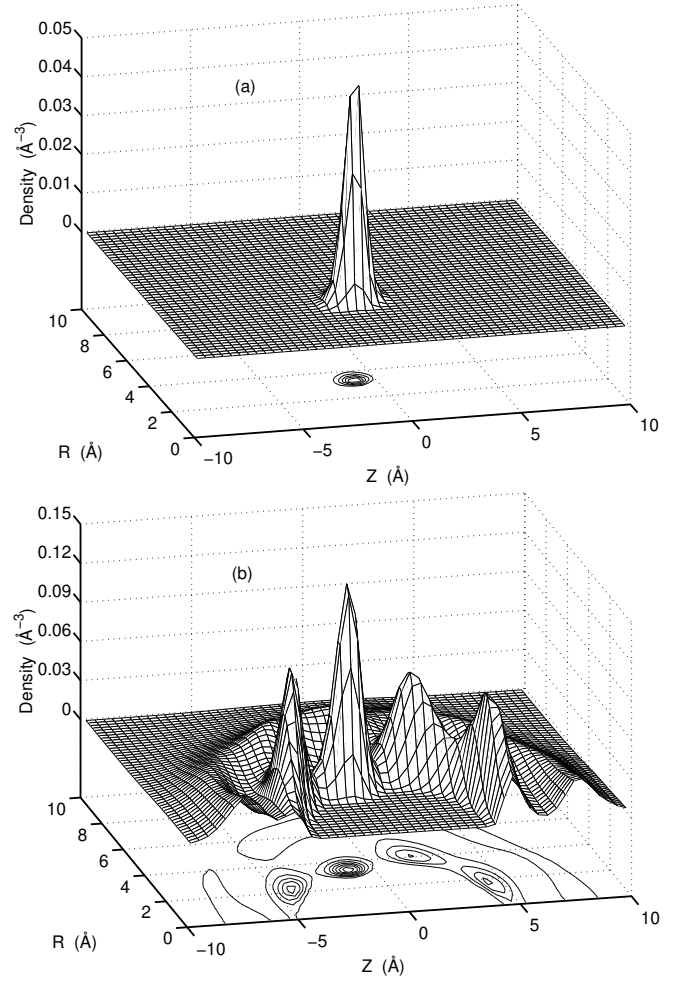


FIG. 4: Density of H_2 and He in the $(\text{OCS-H}_2)^4\text{He}_{63}$ cluster, shown in the cylindrical coordinates Z and R with origin at the OCS center of mass (see Figure 1).

integral densities for H_2 provides a highly accurate description of the free OCS-H_2 complex. We note also that the quantum averages are consistent with a simple ball-and-stick model, although the large size of the quantum fluctuations render this model of limited applicability beyond confirming the average structures.

IV. STRUCTURE AND ROTATIONAL CONSTANTS OF OCS-H_2 EMBEDDED IN HELIUM

Figure 4a shows the density distribution of the single H_2 when the OCS-H_2 complex is now embedded in a cluster of $N = 63$ helium atoms. The corresponding helium density is shown in Figure 4b. Note that the origin in all figures is set to be at the OCS center of mass. The hydrogen distribution is seen to change very little as a result of the surrounding helium atoms (compare Figure 4a with Figure 2), except that the single density peak is somewhat sharper in the presence of helium.

This reflects that the presence of the neighboring helium atoms makes the binding of the hydrogen to the OCS more compact. The average location of the H_2 molecule is now $r = 3.59 \pm 0.31 \text{ \AA}$, $\theta = 105.8 \pm 7.5^\circ$, very similar to its location in the free complex. This location compares well with the values $r = 3.9 \pm 0.2 \text{ \AA}$, $\theta = 111 \pm 6^\circ$ extracted from the spectroscopic measurements in Ref. 10. The close similarity of the structure of the $OCS-H_2$ complex with and without solvating helium suggests that the rigid coupling of the hydrogen to OCS remains a valid approximation when the complex is embedded in helium.

Looking closely now at the helium distribution, it is evident that the first shell structure of this looks very similar to the corresponding first shell structure for the OCS^4He_6 cluster (see Figure 3 of Ref. 26), with one significant difference. This is that the most intense density peak at the global minimum consists now of only five helium atoms, instead of the six helium atoms seen for OCS^4He_6 . This difference is due to the fact that one helium atom is now replaced by a more strongly-bound H_2 molecule. Related calculations with larger numbers of hydrogen molecules have shown that the six helium atoms located at the global minimum in OCS^4He_N are completely replaced by five hydrogen molecules.³⁴ (Similar conclusions have been recently reached from an intensity analysis of spectral lines in Ref. 35.)

In order to estimate the rotational constants of the $OCS-H_2$ complex inside the larger helium droplets, we use the microscopic two-fluid theory of the response of the solvating helium density to the molecular rotation.^{13,17} First, we investigate the local perturbation of helium superfluidity around the $OCS-H_2$ complex, using the local superfluid estimator based on the exchange length of the Feynman paths. As in our previous study for the SF_6 - and OCS -doped helium droplets,¹³ we choose an exchange length of six or greater as the criterion for paths contributing to local superfluidity at any given position. The results are relatively insensitive to this cutoff length, since the paths are generally split between very small paths (2-5 exchanges) and very long paths ($> N$ exchanges).

The moment of inertia tensor of the complex inside the helium droplet is then evaluated by summing the rigidly-coupled single hydrogen and the solvating helium contributions to the gas-phase moment of inertia tensor of OCS:

$$I_{ij} = [I_0]_{ij} + [I_{H_2}]_{ij} + [I_{He}]_{ij}; \quad (7)$$

where the hydrogen contribution I_{H_2} is given by the second term in Eq. (6). We employ here the body-fixed frame of the free $OCS-H_2$ complex defined with origin on the OCS center of mass (see Section III). This is consistent with the reference frame employed in the analysis of the experimental measurements in Ref. 10.

Within the local two-fluid approach the helium contribution can be estimated by

$$[I_{He}]_{ij} = m_{He} \int n_s(\mathbf{r}) (r^2_{ij} - x_i x_j) d\mathbf{r}; \quad (8)$$

where $n_s(\mathbf{r})$ is the local helium non-superfluid density. This is defined as

$$n_s(\mathbf{r}) = n(\mathbf{r}) - n_s(\mathbf{r}); \quad (9)$$

where $n(\mathbf{r})$ is the total number density of helium and $n_s(\mathbf{r})$ the local superfluid density estimate obtained by using the long exchange length criterion. In our previous studies of the rotational constants of impurity molecules such as OCS inside pure helium-4 clusters, the molecule-induced non-superfluid fraction is localized essentially in the first shell region.^{13,17} Any non-superfluid density in the second shell was seen to result from cluster finite size effects and decreases as the cluster size increases.¹³ However, in this case of the $OCS-H_2$ complex, the presence of the hydrogen molecule may induce an additional non-superfluid fraction in the second shell region around the OCS. We can determine the extent of this effect by comparing the local non-superfluid helium density in the vicinity of the H_2 molecule for $(OCS-H_2)^4He_6$ with the local non-superfluid density in the corresponding regions for OCS^4He_6 . Figures 5 (a) and (b) show the non-superfluid helium density distributions of $N = 63$ helium atoms around the $OCS-H_2$ complex and of $N = 64$ helium atoms around the OCS molecule, respectively. There is a clear increase in the non-superfluid density in the second helium solvation shell around the $OCS-H_2$ complex in the vicinity of the H_2 molecule. This small region of second shell non-superfluid density is evidently due to the presence of the distinguishable hydrogen molecule nearby.

In our two-fluid estimate of the effective moment of inertia, both this additional non-superfluid fraction in the second shell and the non-superfluid fraction of the helium in the first solvation shell are assumed to be rigidly coupled to the rotation of the complex. For computational convenience, we further assume that the additional non-superfluid fraction in the second shell lies in the instantaneous plane including the linear OCS molecule and the single hydrogen molecule. This allows the second shell contribution to be estimated from integration over the density difference between Figures 5 (a) and (b). Note that this provides an azimuthally averaged value for the second shell non-superfluid density. More realistically, we expect this density to be localized in three dimensions around the instantaneous H_2 azimuthal position. Such a three-dimensional distribution will not necessarily be accurately described by an azimuthal average. However, sampling the relative azimuthal positions of the H_2 and local non-superfluid helium density is computationally extremely expensive, so we have restricted ourselves to the azimuthally averaged approximation here, bearing in mind that this may lead to some inaccuracy in the second shell contribution to the moment of inertia tensor because of the inaccuracy of the underlying mass distribution. The effective moment of inertia tensor of Eq. (7) is then diagonalized to yield the principal axes of the hydrogen complex in helium, \hat{a} , \hat{b} , and \hat{c} , and the principal moments of inertia tensor I_a , I_b , and I_c .

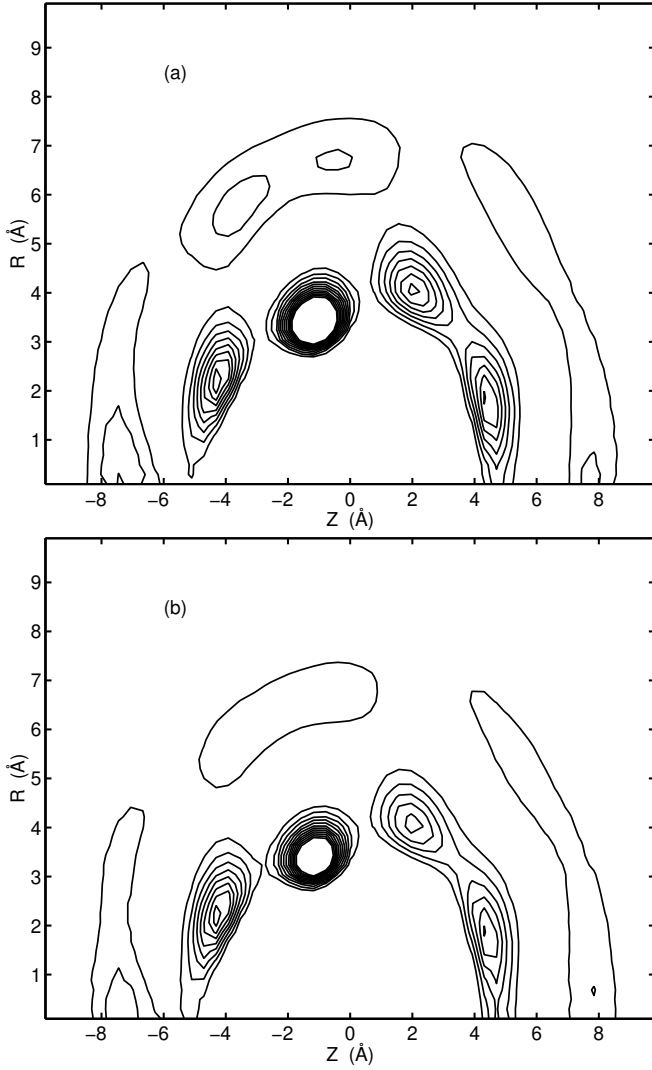


FIG. 5: Non-superfluid helium density around (a) the OCS-H_2 complex in $(\text{OCS-H}_2)^4\text{He}_{63}$, and around (b) OCS in $\text{OCS}^4\text{He}_{64}$. The densities are shown in mesh plots with contours below, in the cylindrical coordinates Z, R defined in Figure 1.

Possible contributions from the superfluid are limited by angular momentum and adiabatic following constraints, as discussed in detail in Ref. 17, and are consequently very small. A recent angular-momentum-consistent calculation for bare OCS in helium has confirmed that the superfluid contribution is negligible in this case,³⁶ and this is expected to be the same for the OCS-H_2 complex.

The resulting moments of inertia and principal axis angle are listed in Table II. The average of the three PIMC principal moments of inertia is in excellent agreement with the experimentally derived average (to 4%), lying within the statistical error of the path integral estimate. However we note that the PIMC estimates for three principal values of the moment of inertia differ from their corresponding experimental values I_a , I_b , and I_c ,

TABLE II: PIMC moments of inertia (in amu \AA^2), and principal axis angle of the OCS-H_2 complex inside a $^4\text{He}_{63}$ cluster, compared with the corresponding experimental values obtained from spectroscopic measurements in large helium droplets ($N \approx 10^3$).¹⁰

	PIMC	Expt.
I_a	246 (12)	199 (1)
I_b	328 (14)	297 (3)
I_c	352 (14)	399 (6)
$(I_a + I_b + I_c)/3$	309 (13)	297 (4)
	7.5	39 (2)

by +23%, +10% and 11%, respectively. There are two possible contributions to these individual discrepancies. First, as discussed above the local superfluid estimator based on exchange path length does not reflect the tensorial nature of the superfluid response, and consequently it may not distinguish effectively among the three principal axes \hat{a} , \hat{b} and \hat{c} . Second, as noted above, we have approximated the contribution from the second helium solvation shell as deriving from a non-superfluid density restricted to the OCS-H_2 plane. Small inaccuracies in the second shell non-superfluid mass distribution resulting from this approximation may give rise to errors in the estimated contribution of this shell to the moment of inertia tensor. The fact that the individual principal moment of inertia values are not achieved at the same accuracy as the average value, indicates that the mass distribution in the second shell is not predicted with sufficient accuracy from our simple estimate based on the azimuthally averaged non-superfluid density. The difference between the experimental value of the principal axis angle and the PIMC estimate of this seen in Table II can also be understood to result from this effect, since like the individual moments of inertia, derives from diagonalization of the moment of inertia tensor. Finally, any inaccuracy in the individual values of I_a , I_b , and I_c will propagate to the estimate of the inertial defect $\Delta I = I_c - I_a - I_b$. We obtain a value $\Delta I = -222 \text{ amu \AA}^2$. This is negative, in agreement with the experimental finding in Ref. 10 and implying a non-planar effective complex in helium,³⁷ but is larger in magnitude than the experimental value $\Delta I = 100 \text{ amu \AA}^2$. This discrepancy is also consistent with the 10 - 23% inaccuracy in the individual moment of inertia values deriving from the effect of using an approximate mass distribution from the second helium solvation shell.

In order to assess the importance of the second-shell helium contribution to the moment of inertia of the complex, we show in Table III the various contributions to the moments of inertia, namely, from the H_2 density and from the non-superfluid helium density in the first and second solvation shells, respectively. As can be seen, the second-shell helium contribution is quite significant, amounting to 18% of the first-shell helium contribu-

TABLE III: The moments of inertia (in $\text{amu}\text{\AA}^2$) contributions from the rigidly-coupled hydrogen (OCS-H_2), the first-shell non-superfluid of helium (He I), and the second-shell non-superfluid of helium (He II), respectively.

	OCS-H_2	He I	He II
I_a	22.82	182	41
I_b	86.10	219	23
I_c	108.92	200	43
$(I_a + I_b + I_c)=3$	72.61	200	36

TABLE IV: PIMC rotational constants (in cm^{-1}) of the OCS-H_2 complex inside a $^4\text{He}_{63}$ cluster, compared with the corresponding experimental values obtained from spectroscopic measurements in large helium droplets ($N=10^3$).¹⁰

	PIMC	Expt.
A	0.069 (4)	0.0847 (4)
B	0.051 (3)	0.0567 (6)
C	0.048 (3)	0.04226 (6)
$(A + B + C)=3$	0.056 (3)	0.04948 (6)

tion to the average moment of inertia of the complex. We find that if the contributions from the second solvation shell are omitted (OCS-H_2 column plus He I column in Table III), the average moment of inertia differs from the experimental quantity by a greater amount, namely 8%, while the individual principal moments of inertia differ now from experiment by +3%, +2% and 23%, respectively. The fact that the average moment of inertia is now significantly lower and in poorer agreement with the corresponding experimental value confirms the need to take the second shell non-superfluid contribution into account.

Since we calculate directly the moment of inertia tensor of the OCS-H_2 complex, a comparison of the principal moments of inertia with corresponding experimental values is the best way for us to calibrate our accuracy. Assessment of the resulting rotational constants is also possible, but is complicated by the need to invert the principal values and the consequent increase in error. Table IV shows the comparison of the PIMC rotational constants and the corresponding experimental values. Even though the average rotational constant is less accurate than the average principal moment of inertia, the PIMC-based estimate for the average rotational constant is still in good agreement with the experimental value, to 15%. Given the approximate description of the second shell helium contribution, this would appear to be excellent agreement.

V. DISCUSSION

We have presented microscopic quantum calculations of the rotational constants of OCS-H_2 both as a free complex and when embedded in helium droplets. The analy-

sis was based on path integral calculations, and employed an assumption of rigid coupling of the H_2 motion to the OCS rotation, as well as the microscopic local two-body theory to evaluate the helium contribution to the moment of inertia. The OCS-H_2 complex is found to be an asymmetric rotor, and to possess a very similar structure when free and when embedded in helium. The complex is seen to induce a local non-superfluid helium density in the second solvation shell, in the immediate vicinity of the H_2 molecule, as well as in the first shell. The overall effect of the solvating helium is to change the complex geometry as measured spectroscopically, from planar to non-planar, reflecting an additional moment of inertia contribution from the solvating helium. The calculated moments of inertia derived from the two-body estimates and corresponding rotational constants are in excellent agreement with experimentally measured values for the free OCS-H_2 complex, with individual values within 3%. For the OCS-H_2 complex embedded in a helium cluster, the average moment of inertia is in excellent agreement with the corresponding experimental average, within 4%, when the contribution from the non-superfluid density induced by the H_2 molecule in the second solvation shell of helium is taken into account. The individual values of the moments of inertia have larger deviations from experiment, 10–23%, but are still in good agreement. These individual deviations, as also the deviation in angle and in magnitude of inertial defect may derive from inaccuracies in the components of the moment of inertia tensor resulting from treating the second shell helium contribution as azimuthally symmetric.

The two-body analysis made here provides a physically consistent explanation of the anomalous effective masses assigned to the H_2 molecule in the extended shell model proposed in Ref. 10. In that model, an extension of the earlier donut model for OCS in helium droplets,³⁸ the increased moment of inertia was assigned to contributions from H_2 and from non-superfluid helium in the first solvation shell only. The latter was estimated from a close packing model of our PIMC helium density distributions,¹⁷ with effective helium masses of 0.55 amu assigned to approximate the theoretical non-superfluid density. The contribution from the H_2 molecule was described with an adjustable effective mass parameter, whose best fit value to experiment was 10 amu.¹⁰ This large increase in effective mass of H_2 was attributed in Ref. 10 to the substitution of one indistinguishable helium atom by a distinguishable H_2 molecule, without any associated change in the surrounding helium density distribution. The analysis made here provides a simpler and more physical explanation for the anomalously large effective mass of H_2 , namely, that this necessarily results when the H_2 -induced second shell non-superfluid density is neglected and the moment of inertia increment is assumed to result only from the first solvation shell density components. The fitted value of the H_2 effective mass is larger than its natural mass because this adjustable parameter must absorb the second shell contributions in

the extended shell model of Ref. 10. It is therefore identified as an artifact of the model that would be removed if the model were extended to include the second shell helium contribution.

A rigid coupling of the hydrogen molecule to rotation of a heavy molecule such as OCS seen here is not unexpected. Related studies have shown that this description becomes less accurate for higher total angular momentum states of the complex.¹⁶ It is useful to compare this behavior of the OCS-H₂ complex with that of its cousin, the OCS-He complex, which is considerably less rigid (see, e.g., the comparative analysis in Ref. 16). Despite having similar topology of interaction potentials, the H₂ molecule has considerably stronger binding to OCS than does He. This results in a more sharply modulated structure, less delocalization, and more rigidity in coupling of its density to the OCS motion, reflecting the presence of low lying excitations of a rigid complex. Nevertheless, it is important to realize that the hydrogen component is still a highly quantum element and this becomes very evident for larger M (see below).

The excellent agreement with a rigid coupling model for the free complex suggests that similar rigid coupling, or more general quasi-adiabatic coupling,^{16,39} descriptions might provide good approximations for the analysis of OCS(H₂)_M, both free and embedded in helium droplets. However, at larger sizes, in particular for M > 11, we have recently shown that the hydrogen component possesses an anisotropic superfluid state.⁹ This state is by definition characterized by a lack of rigid response to rotation about the molecular axis. The first solvation shell is complete at M = 17, and at intermediate M values one can identify precursors to the superfluid state that possess significant permutation exchanges within certain segments of the local solvation structure.⁹ Thus for intermediate sizes one expects the values of rotational constants to reflect a balance between rigidity due to the strong OCS-H₂ and H₂-H₂ interactions, and lack of rigidity due to onset of these permutation ex-

changes. The intermediate-size hydrogen complexes with OCS provide a rich opportunity to analyze the detailed evolution from full rigidity to anisotropic rigidity and superfluidity.

The high accuracy of this two-fluid analysis for the moments of inertia and rotational constants of the OCS-H₂ complex when embedded in helium provides confirmation of the accuracy of the underlying local two-fluid theory. This analysis of moments of inertia and rotational constants for OCS-H₂ inside a helium droplet provides the first microscopic quantum calculation of rotational constants for a van der Waals complex inside helium. The average values are found to be highly accurate, and the slightly larger deviations for the individual values understandable in terms of simplifications of the helium non-superfluid density made here to allow computational tractability. The present analysis thereby extends the previous findings of highly accurate two-fluid calculation of rotational constants for the isolated molecules SF₆ and OCS in helium clusters^{13,17} to embedded molecular clusters. In the case of these heavy molecules and clusters for which high quality interaction potentials are available to enable meaningful microscopic calculations to be made, the two-fluid theory thus appears to provide an accurate microscopic description of response of a solvating superfluid helium droplet to the molecular rotation.

V I. ACKNOWLEDGMENTS

This work has been supported by the Korea Science & Engineering Foundation through its Basic Research Program (grant R01-2002-000-00326-0 to YK) and by the Chemistry Division of the National Science Foundation (grant CHE-0107541 to KBW). KBW thanks the Miller Institute for Basic Research in Science for a Miller Research Professorship for 2002{2003.

- ¹ J. P. Toennies, A. F. Vilesov, and K. B. Whaley, *Physics Today* 54, 31 (2001).
- ² T. E. Gough, M. Mengel, P. A. Rowntree, and G. Scoles, *J. Chem. Phys.* 83, 4958 (1985).
- ³ K. Nauta and R. E. Miller, *Science* 287, 293 (2000).
- ⁴ A. Bartelet, J. D. Close, F. Federmann, N. Qaas, and J. P. Toennies, *Phys. Rev. Lett.* 77, 3535 (1996).
- ⁵ F. Federmann, K. Homan, N. Qaas, and J. P. Toennies, *European Physical Journal D* 9, 11 (1999).
- ⁶ K. Nauta, D. T. Moore, P. L. Stiles, and R. E. Miller, *Science* 292, 481 (2001).
- ⁷ K. Nauta and R. E. Miller, *Science* 283, 1895 (1999).
- ⁸ S. Grebenev, B. Sartakov, J. P. Toennies, and A. F. Vilesov, *Science* 289, 1532 (2000).
- ⁹ Y. Kwon and K. B. Whaley, *Phys. Rev. Lett.* 89, 273401 (2002).
- ¹⁰ S. Grebenev, B. G. Sartakov, J. P. Toennies, and A. F. Vilesov, *J. Chem. Phys.* 114, 617 (2001).
- ¹¹ S. Grebenev, E. Lugovoi, B. G. Sartakov, J. P. Toennies, and A. F. Vilesov, *Faraday Discussions* 118, 19 (2001).
- ¹² J. Tang and A. R. W. McKellar, *J. Chem. Phys.* 116, 646 (2002).
- ¹³ Y. Kwon and K. B. Whaley, *Phys. Rev. Lett.* 83, 4108 (1999).
- ¹⁴ F. Paesani, F. A. Gianturco, and K. B. Whaley, *J. Chem. Phys.* 115, 10225 (2001).
- ¹⁵ K. Higgins, Z. Yu, and W. H. Klemperer, p. to be published (2003).
- ¹⁶ R. Zillich and K. B. Whaley, *Chem. Phys.* p. in press (2003).
- ¹⁷ Y. Kwon, P. Huang, M. V. Patel, D. Blume, and K. B. Whaley, *J. Chem. Phys.* 113, 6469 (2000).
- ¹⁸ M. A. McMahon, R. N. Barnett, and K. B. Whaley, *J. Chem. Phys.* 104, 5080 (1996).

- ¹⁹ P. Huang, Y. Kwon, and K. B. Whaley, in *Quantum Fluids in Confinement*, edited by E. Krotschek and J. Navarro (World Scientific, Singapore, 2002), vol. 4 of *Advances in Quantum Many-Body Theories*, physics/0204089.
- ²⁰ M. V. Patel, A. Viel, F. Paesani, P. Huang, and K. B. Whaley, *J. Chem. Phys.* (2003).
- ²¹ R. Zillich, Y. Kwon, and K. B. Whaley, to be published (2003).
- ²² L. C. van den Bergh and J. A. Schouten, *J. Chem. Phys.* 89, 2336 (1988).
- ²³ R. A. Aziz, F. R. W. McCourt, and C. C. K. Wong, *Mol. Phys.* 61, 1487 (1987).
- ²⁴ K. Higgins and W. H. Klemperer, *J. Chem. Phys.* 110, 1383 (1999).
- ²⁵ D. M. Ceperley, *Rev. Mod. Phys.* 67, 279 (1995).
- ²⁶ Y. Kwon and K. B. Whaley, *J. Chem. Phys.* 114, 3163 (2001).
- ²⁷ E. L. Pollock and D. M. Ceperley, *Phys. Rev. B* 36, 8343 (1987).
- ²⁸ D. M. Ceperley and E. L. Pollock, in *Monte Carlo Methods in Theoretical Physics*, edited by S. Caracciolo and A. Fabbrocini (ETS Editrice, Pisa, Italy, 1992).
- ²⁹ P. Sindzingre, M. L. Klein, and D. M. Ceperley, *Phys. Rev. Lett.* 63, 1601 (1989).
- ³⁰ E. Draeger and D. Ceperley, *Phys. Rev. Lett.* 90, 065301 (2003).
- ³¹ BOUND, computer code version 5, distributed by collaborative computational project no. 6 of the science and engineering research council (u.k.).
- ³² N. Hunt, S. C. Foster, J. W. C. Johns, and A. R. W. McKellar, *J. Mol. Spectrosc.* 111, 42 (1985).
- ³³ G. D. Hayman, J. Hodge, B. J. Howard, J. S. Muentert, and T. R. Dyke, *J. Mol. Spectrosc.* 133, 423 (1989).
- ³⁴ M. Patel, *Faraday Discussions* 118, 47 (2001).
- ³⁵ S. Grebenev, B. G. Sartakov, J. P. Toennies, and A. F. Vilesov, *Phys. Rev. Lett.* 89, 225301 (2002).
- ³⁶ P. Huang, T. Sachse, and K. B. Whaley, to be published (2003).
- ³⁷ W. Gordy and R. L. Cook, *Microwave Molecular Spectra* (Wiley Interscience, New York, 1984).
- ³⁸ S. Grebenev, M. Hartmann, M. Havenith, B. Sartakov, J. P. Toennies, and A. F. Vilesov, *J. Chem. Phys.* 112, 4485 (2000).
- ³⁹ M. Quack and M. A. Suhm, *J. Chem. Phys.* 95, 28 (1991).